JOURNAL OF CRITICAL REVIEWS

ISSN- 2394-5125 VOL 7, ISSUE 06, 2020

Structure analysis of 6-aminonicotinic acid from a sample containing an additional crystalline phase using laboratory and synchrotronX-ray powder diffraction data

Tanusri Dey[1*] and Alok Kumar Mukherjee[2]

1 School of Applied Science and Humanities, Haldia Institute of Technology, India

2 Institute of Business Management, National Council of Education –Bengal, India

ABSTRACT

The crystal structure of 6-amino nicotinic acid (6-ANA) which is a derivative of vitamin B3, was determined from a sample having an additional crystalline phase using both laboratory and synchrotron X-ray powder diffraction data. The nature of intermolecular interactions in 6-ANA has been analysed through Hirshfeld surfaces and 2-dimensional fingerprint plots and compared with those in some other nicotinic acid derivatives.A pair of intermolecular N–H···O and O–H···N hydrogen bonds generated cyclic $R^2_2(8)$ rings in 6-ANA forming one dimensional molecular strips, which are further connected through N–H···O hydrogen bonds to produce a three dimensional supramolecular framework. Geometry optimization of 6-ANA was carried out along with the molecular electrostatic potential calculations. The enrichment ratio of various contacts, calculated for 6-ANA and some other related compounds retrieved from the CSD, show an increased propensity of O···H and N···H contacts to form, which is consistent with the intermolecular interactions, found from crystallographic studies.

Keywords: 6 Amino nicotinic acid, Hirshfeld surface analysis, Powder diffraction, Qualitative phase analysis, Solid state DFT

1. Introduction

Nicotinic acid (pyridine-3-carboxilic acid) or NA, also known as niacin or vitamin B_3 is an essential human nutrient used to treat high blood cholesterol. Deficiency of NA in regular diet can cause nausea, skin and mouth lesions, anemia, headaches, and tiredness. NA and its derivatives are of considerable importance due to their biochemical properties [1-4]. While 6-methylnicotinic acid (a derivative of NA) is used as an intermediate during the synthesis of etoricoxib, a non- steroidal anti-inflammatory drug for treating arthritis and osteoarthritis [5], the corresponding dimethoxymethyl derivative of NA and its sodium salt can act as an organogeletor [6]. Several chloro compounds containing NA are important ingredients for agrochemicals, feed additives, animal food enrichment and pharmaceuticals [7]. 6-aminonicotinic acid (6-ANA), a structural analogue of p-amino benzoic acid, is known to produce bacteriostasis in Escherichia coli and streptococcus haemolyticus and it also inhibits multiplication of T2 bacteriophage [8. 9]. 6-ANA, a main constituent of vitamin B_3, is also used to cure pellagra disease [10]. It is surprising to note that the compound 6-ANA in spite of its potential biological significance has not been structurally characterized till date using X-ray diffraction. The spectroscopic and structural analysis of 2-ANA has been, however, reported in the literature [11, 12].

In this paper, the crystal structure analysis of 6-ANA (**I**) using powder X-ray diffraction is presented. Although single crystal Xray diffraction (XRD) is the method of choice for determining structure of molecular compounds, but there are limitations in this process due to the unavailability of single crystal of adequate size and quality and ab-initio structure determination from powder X-ray diffraction is a far more difficult task than that of its single-crystal counterpart.In spite of that, with recent advances in the direct space approaches for structure solution [13-16], ab-initio crystal structure determination from powder X-ray diffraction (PXRD) has been reported for organic systems with considerable molecular flexibility [17-20]. It should, however, be noted that the success of ab-initio structure solution from PXRD is highly dependent on the purity of the sample i.e. the material should be a single-phased one. The complexity of ab-initio structure solution from PXRD increases by many folds when the material contains multiple crystalline phases. The present paper reports a successful attempt of structure solution from PXRD for a sample containing 6-ANA as the major phase and some unknown minor phase(s). DFT calculations were also carried out to confirm the molecular geometry of 6-ANA and

ISSN- 2394-5125 VOL 7, ISSUE 06, 2020

analyze the electronic structure. An investigation of close intermolecular interactions in **I**, NA and a few related substituted NA derivatives via Hirshfeld surface analysis is also presented.

2: Experimental

2.1: Source

The compound 6-ANA (I) was purchased from Sigma Aldrich with CAS no. 3167-49-5 and used without any further purification.

2.2: In-house X-ray data collection

Powder X-ray diffraction (PXRD) data of **1** were recorded in-house at ambient temperature [293 (2) K] on a Bruker D8 Advance diffractometer operating in the Bragg−Brentano geometry using CuKα radiation (λ = 1.5418 Å) with a step size (2θ) of 0.02° and a scan speed of 4 sec per step.

2.3: Indexing and structure solution from laboratory PXRD

The powder XRD pattern was indexed using the first 20 peaks with the NTREOR code [21] in the program EXPO-2014 [22] which resulted in an orthorhombic unit cell. Given the volume of unit cell and consideration of density, the number of formula units (Z) in the unit cell turned out as 4. Statistical analysis of PXRD data using the FINDSPACE module of EXPO 2014 indicated $Pna2_1$ as the most probable space group, which was used for structure solution. The unit cell parameters and space group assignments were validated by a Le-Bail fit of PXRD data using a pseudo-Voigt peak profile function [23]with FOX. The structure solution was carried out by global optimization of molecular models in direct space based on a Monte-Carlo search using the simulated annealing technique in parallel tempering mode as implemented in the program FOX[14]. The initial molecular geometry input to FOX was optimized by an energy gradient method as incorporated in the MOPAC 9.0 program [24].

2.4: Refinement using laboratory PXRD data

The best structural model i.e. the structure with lowest R_{wp} was used as the input for Rietveld refinement [25] using the program GSAS [26]. A pseudo-Voigt peak profile function was used during refinement and the background of the PXRD pattern was modeled by a shifted Chebyshev function of the first kind with 30 points regularly distributed over the entire 2θ range. The profile parameters were refined initially followed by the refinement of positional coordinates of all non-hydrogen atoms. Standard restraints were applied to bond lengths and bond angles, and a planar restraint was used for the pyridine ring. In the final stage of refinement, a preferred orientation correction using the generalized spherical harmonic model was applied. Hydrogen atoms were placed at the calculated positions and their coordinates were held fixed. Once the refinement converged, it was noticed that two relatively weak peaks (with less than 10% of the highest intensity) around 2θ values of 31.75 ° and 45.48 °, respectively, in the PXRD pattern had no corresponding calculated positions (Fig. 1).

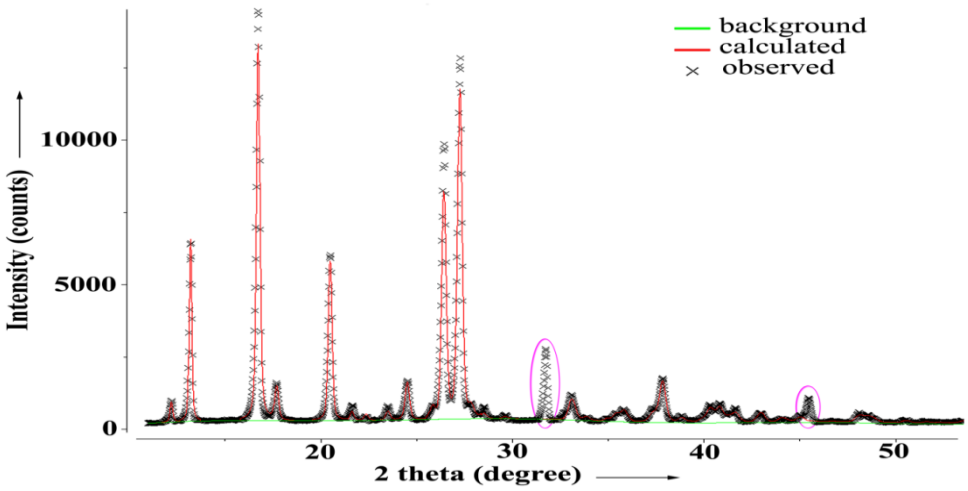

Fig. 1: PXRD pattern of $C_6H_6N_2O_2$ (I); peaks marked in pink circles have no calculated positions

ISSN- 2394-5125 VOL 7, ISSUE 06, 2020

These two weak peaks, however, did not affect our indexing results as only the first 20 peaks (upto 2θ = 30.0 °) were considered during the powder pattern indexing and subsequent analysis of structure solution using FOX was uneventful. The structure determination of **I** was repeated using the PXRD data collected with synchrotron radiation to crosscheck our findings with the laboratory PXRD data.

2.5: Synchrotron PXRD data collection

The synchrotron X-ray powder diffraction pattern was recorded at the 11-Bm beamline, Advanced Photon Source, Argonne National Laboratory. 11-BM is a bending magnet beamline, equipped with a vertical beam collimator mirror, a double crystal monochromator with a horizontal sagittal focusing second crystal, and a vertical focusing mirror. The powder sample was loaded in a polymide capillary (0.8 mm in diameter) and was spun at 6000 rpm during measurement. The data collection was made simultaneously by a set of 12 LaCl3 scintillation detectors, with 2 ° separation between the neighboring detectors, each using a Si (111) crystal as analyzer. Data were collected at 295 K from -6.5 ° to 28.0 º (2θ) with a step size of 0.001º and a step time of 0.1 s/step using a calibrated wavelength (λ) of 0.459002 Å. Additional details of the experimental setup are given elsewhere [27, 28].

2.6: Indexing and structure solution from synchrotron PXRD

The synchrotron PXRD data of **I** also indicated peaks at 2θ values of 9.34 ° and 13.22 °, with enhanced intensity, which could not be indexed using the standard procedure as described earlier. Incidentally, the synchrotron PXRD data yielded almost identical results as that obtained from the laboratory PXRD data. Following structure solution and refinement of **1** using the synchrotron PXRD data, it was apparent that the peaks at 2θ ~ 9.34 ° and 13.22 ° could be due to some other crystalline phase(s) present in the sample used for data collection. The search/match program EVA (Bruker AXS, Karlsruhe, Germany) and ICDD Database (International Centre for Diffraction Data, PDF2 Release 2003) indicated the presence of NaCl in the sample and the two unindexed peaks in the PXRD pattern correspond to two most intense peaks from (200) and (220) planes of NaCl phase. The first peak i.e. from the (111) plane of NaCl, at 8.08 ° (2θ) in the synchrotron PXRD pattern coincided with the strongest peak of **1** and remained unnoticed earlier. It is interesting to note that those extra peaks disappeared when PXRD data were recollected using the sample recrystallized from distilled water. This fact corroborates with our analysis that the minor phase is NaCl. The structure of **I** could also be solved with the synchrotron PXRD following the same procedure used for laboratory PXRD data.

2.7: Quantitative phase analysis using synchrotron PXRD data

Quantitative phase analysis of the material used for synchrotron PXRD was carried out with GSAS assuming the sample as a mixture of two phases, compound **I** as the major phase and NaCl as the minor phase. Initial refinement was performed with the major phase i.e. compound **I** and subsequently the minor phase i.e. NaCl was introduced. The overall scale factor was refined simultaneously with the individual phase fractions. Following the refinement of background coefficients and the unit cell parameters of NaCl, the profile and preferred orientation parameters of NaCl phase were refined, while the corresponding parameters and the atomic coordinates of all non-hydrogen atoms of **I** were held fixed to their earlier refined values. After convergence of refinement with individual phases, the above-mentioned parameters of both phases, **I** and NaCl, were refined simultaneously. In the final stage of refinement, the isotropic thermal displacement parameters (U_{iso}) of all non-hydrogen atoms of both phases were refined individually. The weight fractions obtained after final convergence were 98.32(1) % for **1** and 1.68(5) % for NaCl. The final Rietveld plot (Fig.2) showed an excellent agreement between the observed synchrotron PXRD profile and the calculated powder diffraction pattern. The molecular view of **I**with atom labeling scheme is shown in Fig. 3. A summary of crystal data and relevant refinement parameters for **I**is listed in TABLE 1.

ISSN- 2394-5125 VOL 7, ISSUE 06, 2020

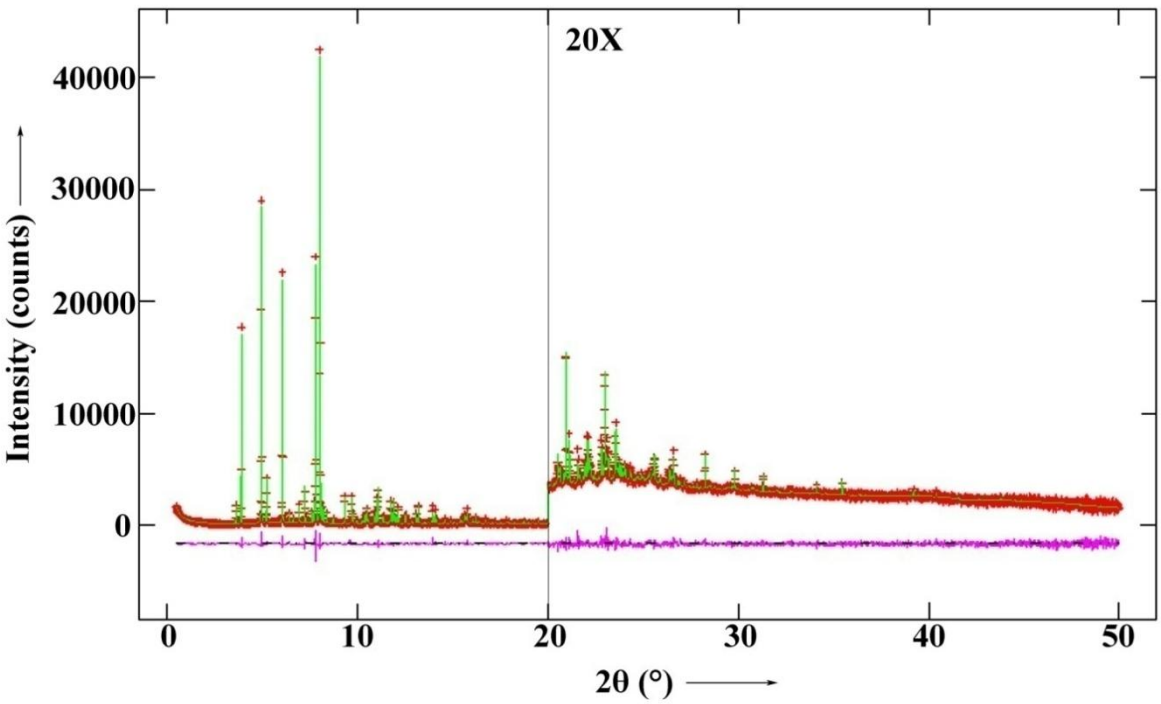

Fig. 2: Powder pattern of $C_6H_6N_2O_2$ (1) (with NaCl) using synchrotron radiation; the high angle region has been zoomed 20 times

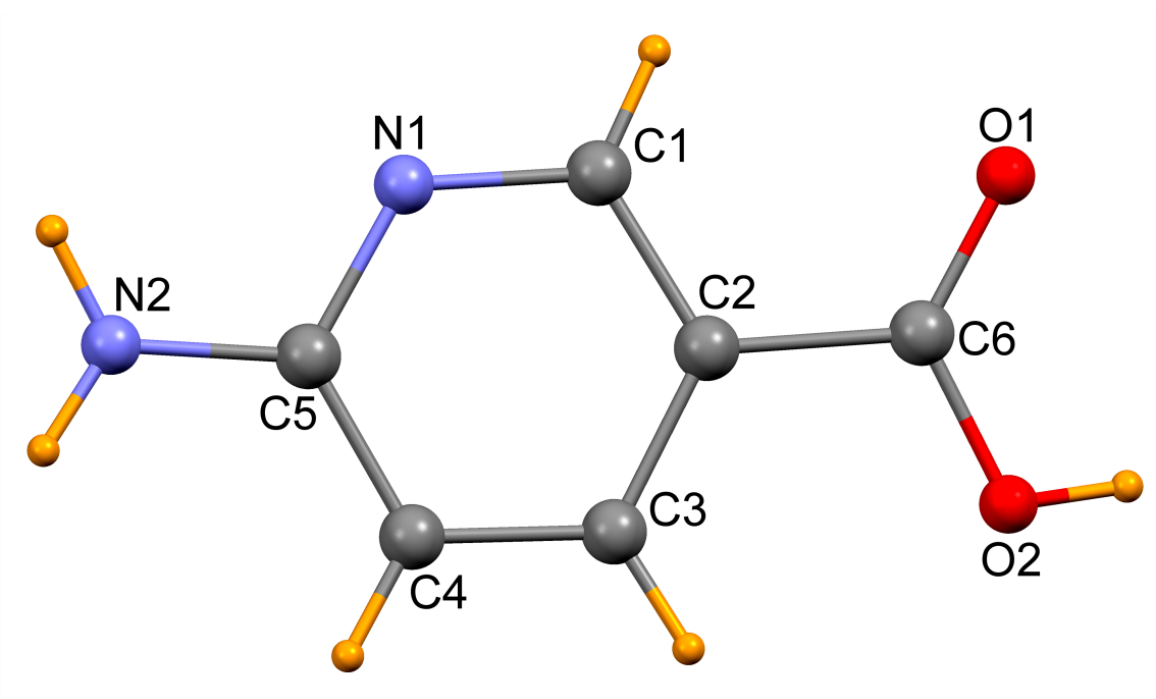

Fig. 3: Molecular view with atom labeling scheme for $C_6H_6N_2O_2$ (I)

Table 1: Crystal data and structure refinement parameters for $C_6H_6N_2O_2$ (I)

Mol. Wt.	138.13	**Density (g/cm^3)**	1.4617(1)
Temperature (K)	295	**μ(mm^{-1})**	0.113
Wavelength (Å)	0.4590020	**No. of variable parameters**	144
Crystal system	Orthorhombic	**No. of background points**	30
a (Å)	8.62688(8)	**Spherical harmonics**	16

ISSN- 2394-5125 VOL 7, ISSUE 06, 2020

b (Å)	13.44382(10)	**R_p**	0.0523
c (Å)	5.41197(5)	**R_{wp}**	0.0766
Volume (Å^3)	627.671(9)	**R(F^2)**	0.0938
Space group, z	Pna2$_1$, 4	**χ^2**	1.708

2.8: Hirshfeld surface analysis

The Hirshfeld surfaces [29-31] and associated 2D fingerprint plots [32-35] were calculated using Crystal Explorer [36]. Bond lengths to hydrogen atoms were set to typical neutron values (C-H = 1.083 Å and N-H = 1.009 Å). For each point on the Hirshfeldisosurface, two distances d_e, the distance from the point to the nearest nucleus external to the surface, and d_i, the distance to the nearest nucleus internal to the surface, are defined. The normalized contact distance (d_{norm}) based on d_e and d_i is given by;

$$d_{norm} = \frac{d_i - r_i^{vdW}}{r_i^{vdW}} + \frac{d_e - r_e^{vdW}}{r_e^{vdW}} \qquad (1)$$

wherer_i^{vdW} and r_e^{vdW} are the van der Waals radii of the atoms. Thevalue of d_{norm} can be negative or positive depending on whetherthe intermolecular contacts are shorter or longer than the van derWaals separations. The parameter d_{norm} displays a surface with ared-white-blue color scheme, where the bright red spots highlight shorter contacts, the white areas represent contacts around the van der Waals separation, and the blue regions are devoid of close contacts.

2.9: Electrostatic potential calculation

The molecular electrostatic potential (MEP) is an effective tool for identifying and ranking the hydrogen bond donating and accepting sites in organic compounds [37. 38]. The electrostatic potential at any point $\vec{r}$ in the space surrounding a molecule can be expressed by

$$V(\vec{r}) = \sum_A \frac{Z_A}{|\overrightarrow{R_A} - \vec{r}|} - \int \frac{\rho(\vec{r}')dr'}{|\vec{r} - \vec{r}'|} \qquad (2)$$

where Z_A is the charge of the nucleus A located at $\overrightarrow{R_A}$ and $\rho(\vec{r})$ is the molecular electron density function. The sign of $V(\vec{r})$ at a particular region depends upon whether the effect of the nucleus or the electrons is dominant there. The MEP surfaces of **1** were generated with BLYP [39, 40] correlation functional and a double numeric plus polarization (DNP) basis set using isolated molecule DFT calculations. All calculations including the electron densities and esp charges were carried out using the Dmol3 code [41]. The starting atomic coordinates for property calculations were obtained by geometry optimization of the structure from the final X-ray refinement cycle in the solid state with the same correlation functional and basis set. The dispersion correction was carried out with DFT-D approach using the TS scheme [42]. The electrostatic potentials were plotted on 0.017 au electron density isosurface [43]. The MEP surfaces have been mapped with a rainbow color scheme with red representing the highest negative potential region while blue representing the highest positive potential region.

3: Results and discussion

3.1: Structure description

The overall molecular conformation in **I**can be described by the relative orientation of carboxyl group as well as the amino group at the para position, with respect to the planar pyridine ring. The amino group displays an almost planar geometry due to the conjugation of lone pair of nitrogen atom with the aryl substituent, as seen in aromatic amines. The H1N2-N2-H2N2 angle for **I** is 117.0 ° which is close to the mean value of 119.4 °, retrieved from the CCDC search of 291 hits for aminopyridines. The C5-N2 bond distance is 1.344(4) Å (TABLE 2) showing a partial double bond characteristic of the C-N bond.

Table 2: Bond lengths (Å) and bond angles (˚) for $C_6H_6N_2O_2$ (I) as obtained from PXRD analysis and DFT calculations

Bonds	**Bond lengths (Å)**		**Angles**	**Bond angles (˚)**	
	PXRD	**DFT**		**PXRD**	**DFT**
O1 - C6	1.207(3)	1.2487	C1 - N1 - C5	123.6(3)	118.59
O2 - C6	1.293(4)	1.3317	N1 - C1 - C2	117.8(2)	123.41

ISSN- 2394-5125 VOL 7, ISSUE 06, 2020

N1 - C1	1.337(4)	1.3376	C1 - C2 - C3	121.0(2)	118.04
N1 - C5	1.343(3)	1.3642	C1 - C2 - C6	117.4(2)	118.97
N2 - C5	1.344(4)	1.3472	C3 - C2 - C6	121.7(2)	122.99
C1 - C2	1.384(4)	1.3918	C2 - C3 - C4	119.2(2)	119.52
C2 - C3	1.399(4)	1.408	C3 - C4 - C5	118.1(2)	119.15
C2 - C6	1.470(4)	1.4587	N1 - C5 - N2	116.7(2)	117.5
C3 - C4	1.384(4)	1.3741	N1 - C5 - C4	120.2(2)	121.29
C4 - C5	1.401(4)	1.415	N2 - C5 - C4	123.0(2)	121.21
			O1 - C6 - O2	124.3(3)	122.52
			O1 - C6 - C2	122.6(3)	121.43
			O2 - C6 - C2	113.1(2)	116.06

The distance of N2 from the mean plane through C5, H1N2 and H2N2 atoms is 0.066 Å, while the mean distance for such aminopyridine structures from CSD is 0.074 Å. On the other hand, the carboxylic acid group is also planar making a dihedral angle of 5.85° with the pyridine plane. The C-N bond distances in the pyridine ring [1.337(4) and 1.343(3) Å] agree well with the mean value [1.340 Å] of partial double bond distances for C-N bonds in the pyridine groups as retrieved from the CSD. In a planar molecule, the torsional angles are either 0° or 180°. The r.m.s. deviation from planarity for torsion angles (TABLE 3) in **I**of 2.16 ° indicates an overall planarity of molecule. An overlay of molecular conformations of the title compound as determined by synchrotron X-ray powder diffraction analysis and theoretical calculations (solid state DFT) is shown in Fig. 4. The r.m.s. deviations of the geometrically optimized bond lengths and bond angles from the corresponding crystallographically determined values are 0.02 Å and 2.6 °, respectively, in**I**. Close agreement between the X-ray analyzed structure and that obtained via quantum-mechanical calculations probably indicates that the compound studied is a stable conformer.

Table 3: Torsion angles (˚) for $C_6H_6N_2O_2$ (1) as obtained from PXRD analysis

Atoms	Torsion angle	Atoms	Torsion angle
C2 -C1-N1-C5	-0.7(4)	C3-C2-C6-O1	-176.2(3)
N1-C1-C2-C3	1.9(4)	C3-C2-C6-O2	4.1(4)
N1-C1-C2-C6	-178.3(3)	C2-C3-C4-C5	0.3(4)
C1-C2-C3-C4	-1.7(4)	C3-C4-C5-N1	0.9(4)
C6-C2-C3-C4	178.5(3)	C3-C4-C5-N2	177.6(3)
C1-C2-C6-O1	4.0(4)	N2-C5-N1-C1	-177.7(3)
C1-C2-C6-O2	-175.7(3)	C4-C5-N1-C1	-0.7(4)

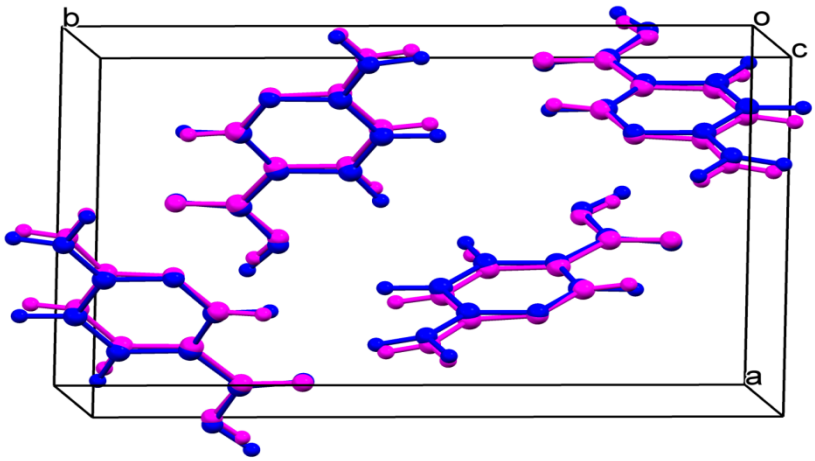

Fig. 4: Superposition of molecular conformation as obtained from synchrotron radiation powder diffraction data (pink) and DFT calculations (blue) for $C_6H_6N_2O_2$ (I)

3.2: Packing

ISSN- 2394-5125 VOL 7, ISSUE 06, 2020

The crystal packing in **I** exhibits an interplay of N-H···O and O-H···N hydrogen bonds (TABLE 4). A pair of intermolecular N2-H1N2···O1 and O2-H1O2···N1 hydrogen bonds connects molecules related by 'a' glide producing a one-dimensional molecular strip (A) formed with $R_2^2(8)$ rings propagating along the [102] direction (Fig.5). Another one-dimensional strip (B) is formed along the [-102] direction when the starting molecule is taken to be that with the screw symmetry [symmetry code: -x, -y, 1/2+z].

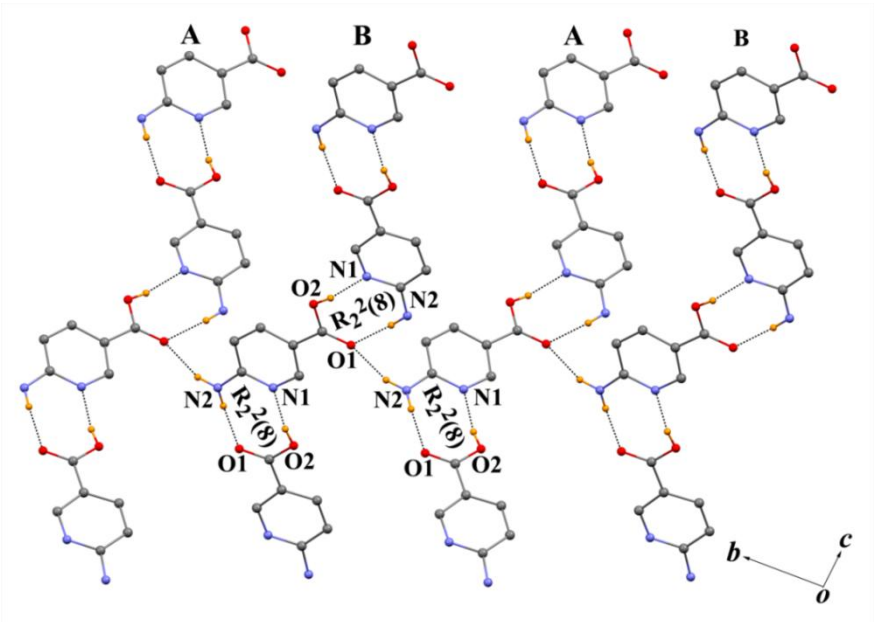

Fig. 5: Formation of two types of chains A and B in $C_6H_6N_2O_2$ (1) by N-H···O hydrogen bonds and their connection by O-H···N hydrogen bonds, projected along the [100] direction

Table 4: Hydrogen bonds in $C_6H_6N_2O_2$ (I)

Interaction	D-H/ Å	H···A/ Å	D···A/ Å	D-H···A/ º	Symmetry code
N2-H1N2···O1	0.86	1.94	2.79894)	173	-1/2+x, 3/2-y, -1+z
N2-H2N2···O1	0.88	1.97	2.814(3)	160	1/2-x, -1/2+y, -1/2+z
O2-H1O2··· N1	0.82	1.93	2.746(4)	171	1/2+x, 3/2-y, 1+z

Two almost perpendicular strips (A and B) are interconnected by N2-H2N2···O1 hydrogen bonds (which individually form $C_2^2(16)$ chains along the [011] direction) producing a three-dimensional cage like structure in **I**(Fig. 6).

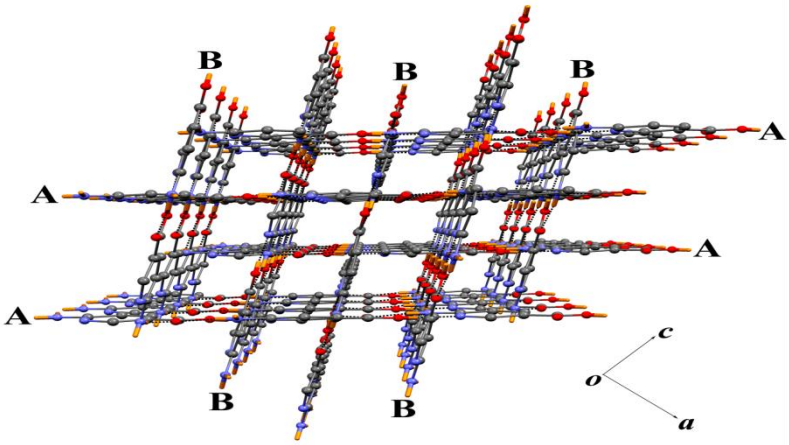

Fig. 6: Formation of three-dimensional cage like structure by two types of chains A and B in $C_6H_6N_2O_2$ (1) produced by N-H···O and O-H···N hydrogen bonds, projected along the [010] direction

ISSN- 2394-5125 VOL 7, ISSUE 06, 2020

3.3: Hirshfeld surface analysis

The Hirshfeld surface of **I** has been illustrated in Fig. 7i showing surface that has been mapped over a d_{norm} range from -0.5 to 1.5 Å. The dominant interactions between the amino hydrogen atoms and the carbonyl oxygen atom can be seen in the Hirshfeld surface of **I** as bright red spots labeled 'a' and 'a′'. Equally bright red spots labeled 'b' and 'b′' in Fig. 7i are attributed to the O-H···N hydrogen bond, where the carboxyl oxygen atom (O1) acts as a hydrogen bond donor to the pyridine nitrogen atom (N1). There is no other significant red spot on the Hirshfeld surface of **I** showing the absence of any other weak intermolecular interaction. In the 2D fingerprint plot (Fig. 7ii) of **I**, two sharp spikes of equal length and labeled as 'a' and 'a′' in the region 2.0 Å $<d_e+d_i<$ 2.4 Å are characteristics of N-H···O hydrogen bonds, while the other two sharp spikes of almost equal length and labeled as 'b' and 'b′' are attributed to the O-H···N hydrogen bond. Absence of any central spike in the 2D fingerprint plot of **I** is a result of long H···H contacts (> 2.52 Å) in **I**.

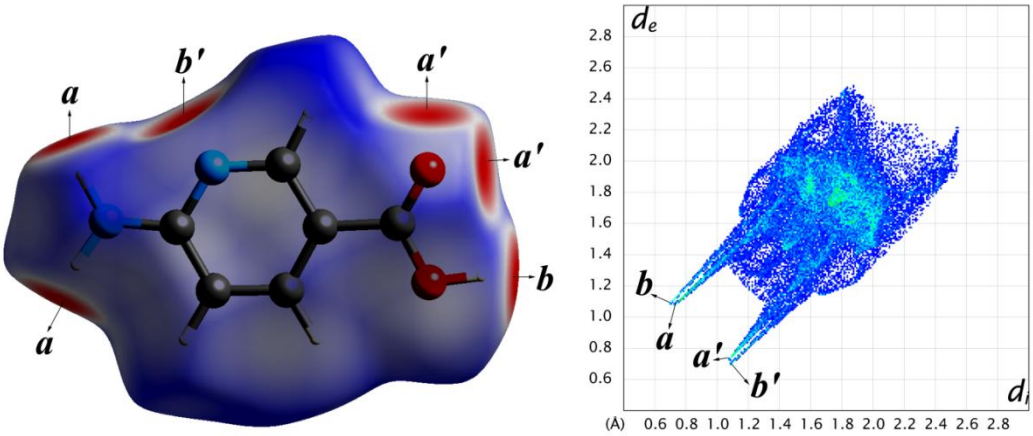

(i) (ii)

Fig. 7: (i) Hirshfeld surface and (ii) fingerprint plot of $C_6H_6N_2O_2$ (I)

The relative contribution of different intermolecular interactions to the Hirshfeld surfaces of **I,** nicotinic acid (NICOAC02) [44] and a few other nicotinic acid derivatives retrieved from the CSD such as 6-(dimethoxymethyl)nicotinic acid (TIZSUR) [6], 6-acetamidonicotinic acid (VIPSUI) [45] and 6-methylnicotinic acid (AYUMUD) [46] is shown in Fig. 8. It is evident from Fig. 8 that H···H, N···H and O···H interactions contribute almost 70% to the Hirshfeld surface area (69.3% in **1**, 72% in NICOAC02, 82.9 % in TIZSUR, 71.6% in VIPSUI A, 70.8% in VIPSUI B and 78.4% in AYUMUD). Due to addition of amino group to the 6-position of nicotinic acid, in **1**, N···H contact steadily increases to 13.2% while the O···H contact reduces to 22% which is the minimum among these compounds (Fig. 8). The contribution of O···H contact is maximum (31.9%) in TIZSUR where the amino group in **I** has been replaced by a dimethoxymethyl group. In **I**, 18.4% contribution comes from the C···H interaction due to large number of intermolecular C···H contacts.

The enrichment ratio (E) [47],i.e. the ratio between the proportion of actual contacts in the crystal and the theoretical proportion of random contacts, has been determined for the intermolecular contacts in **1**, nicotinic acid and the other related structures from CSD (**TABLE 5**) to study the propensity of two chemical species to be in contact. The value of E is greater than unity for pair of elements with higher propensity to form contacts, while pairs which tend to avoid contacts yield E values less than unity. In **1**, the total Hirshfeld surface area is dominated by H···H, O···H, N···H and C···H contacts, comprising of 34.1%, 22.0%, 18.4% and 13.2%, respectively. The corresponding enrichment ratios, however, show an increased propensity of O···H and N···H contacts to form (E_{HO} = 1.16 and E_{HN} = 1.19), which is consistent with the crystallographic results showing strong O···H and N···H intermolecular hydrogen bonds taking part in the packing of **1**. E_{HO} and E_{HN} values are greater than 1 for nicotinic acid and all the other derivatives retrieved from the CSD. However, the H···H contacts are less favored (E_{HH} = 0.92) in **1** as well as the other compounds discussed here. An interesting feature in the compounds (except **1)** is that the enrichment ratios for C···C contacts are very high (3.37 in NICOAC02, 4.57 in TIZSUR, 1.36 in VIPSUI A, 1.28 in VIPSUI B and 3.62 in AYUMUD) due to the presence of very strong π···π interactions, which is absent in **1** (E_{CC} = 0.99).

ISSN- 2394-5125 VOL 7, ISSUE 06, 2020

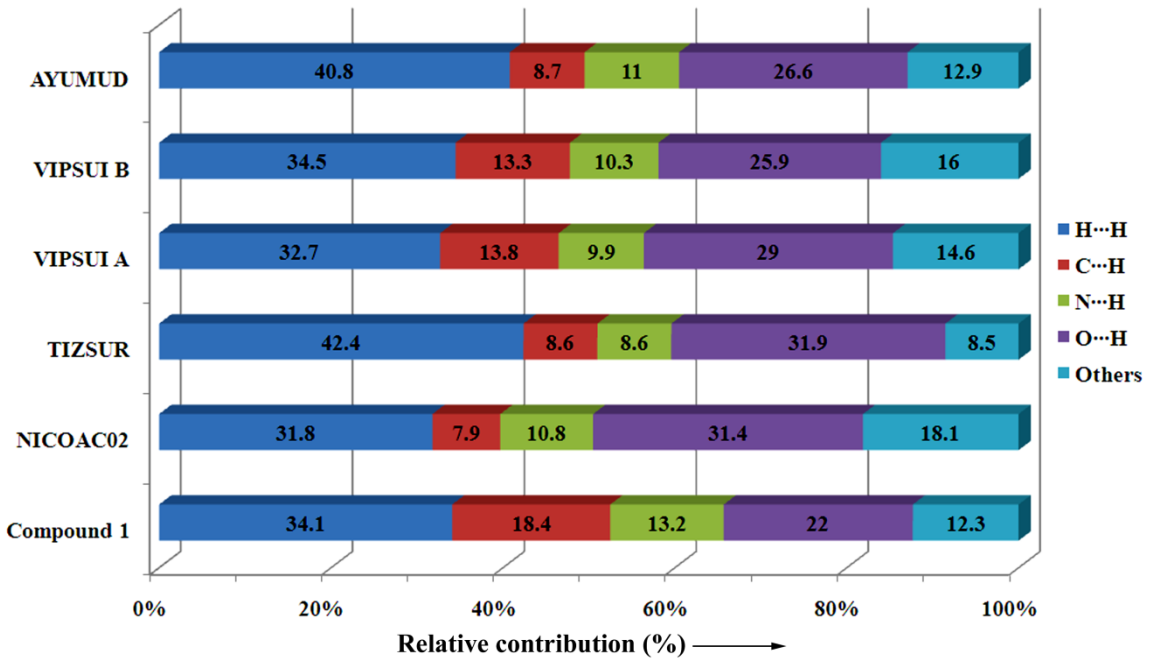

Fig. 6.8: Relative contribution of different intermolecular interactions to the Hirshfeld surfaces of $C_6H_6N_2O_2$ (1), NA and few other NA derivatives retrieved from the CSD

Table 5: Hirshfeld contact surfaces and derived "random contacts" and "enrichment ratios" for $C_6H_6N_2O_2$ (I) and few other compounds retrieved from the CSD

	$C_6H_6N_2O_2$ (1)				NICOAC02				AYUMUD			
	H	C	N	O	H	C	N	O	H	C	N	O
Contacts (C, %)												
H	34.1	18.4	13.2	22	31.8	7.9	10.8	31.4	40.8	8.7	11	26.6
C	18.4	2.1	1.5	5	7.9	10.1	4.9	1.6	8.7	7.3	1.5	3.6
N	13.2	1.5	0	3.5	10.8	4.9	0	0.6	11	1.5	0	0
O	22	5	3.5	0.3	31.4	1.6	0.6	0.9	26.6	3.6	0	0.4
Surface (S, %)												
	60.9	14.55	9.1	15.55	56.85	17.3	8.15	17.7	63.95	14.2	6.25	15.5
Random contact (R, %)												
H	37.09	17.72	11.08	18.94	32.32	19.67	9.27	20.12	40.9	18.16	7.99	19.82
C	17.72	2.12	2.65	4.53	19.67	2.99	2.82	6.12	18.16	2.02	1.77	4.4
N	11.08	2.65	0.83	2.83	9.27	2.82	0.66	2.89	7.99	1.77	0.39	1.94
O	18.94	4.53	2.83	2.42	20.12	6.12	2.89	3.13	19.82	4.4	1.94	2.4
Enrichment (E)												
H	0.92	1.04	1.19	1.16	0.98	0.4	1.17	1.56	1	0.48	1.38	1.34

ISSN- 2394-5125 VOL 7, ISSUE 06, 2020

C	1.04	0.99	0.57	1.1	0.4	3.37	1.74	0.26	0.48	3.62	0.85	0.82
N	1.19	0.57	0	1.24	1.17	1.74	0	0.21	1.38	0.85	0	0
O	1.16	1.1	1.24	0.12	1.56	0.26	0.21	0.29	1.34	0.82	0	0.17

	TIZSUR				**VIPSUI A**				**VIPSUI B**			
	H	**C**	**N**	**O**	**H**	**C**	**N**	**O**	**H**	**C**	**N**	**O**
Contacts (C, %)												
H	42.4	8.6	8.6	31.9	32.7	13.8	9.9	29	34.5	13.3	10.3	25.9
C	8.6	4.9	0.4	1.9	13.8	2.5	1.1	7.2	13.3	2.2	2.3	6.2
N	8.6	0.4	0	0.4	9.9	1.1	0.1	1	10.3	2.3	0.1	3
O	31.9	1.9	0.4	1	29	7.2	1	2.6	25.9	6.2	3	2.4
Surface (S, %)												
	66.95	10.35	4.7	18.1	59.05	13.55	6.1	21.2	59.25	13.1	7.9	19.95
Random contact (R, %)												
H	44.82	13.86	6.29	24.24	34.87	16	7.2	25.04	35.11	15.52	9.36	23.64
C	13.86	1.07	0.97	3.75	16	1.84	1.65	5.75	15.52	1.72	2.07	5.23
N	6.29	0.97	0.22	1.7	7.2	1.65	0.37	2.59	9.36	2.07	0.62	3.15
O	24.24	3.75	1.7	3.28	25.04	5.75	2.59	4.49	23.64	5.23	3.15	3.98
Enrichment (E)												
H	0.95	0.62	1.37	1.32	0.94	0.86	1.37	1.16	0.98	0.86	1.1	1.1
C	0.62	4.57	0.41	0.51	0.86	1.36	0.67	1.25	0.86	1.28	1.11	1.19
N	1.37	0.41	0	0.24	1.37	0.67	0.27	0.39	1.1	1.11	0.16	0.95
O	1.32	0.51	0.24	0.31	1.16	1.25	0.39	0.58	1.1	1.19	0.95	0.6

The enrichment ratios were not computed when the "random contacts" were lower than 0.9%, as they are not meaningful

ISSN- 2394-5125 VOL 7, ISSUE 06, 2020

3.4: Molecular electrostatic potential

The MEP surface of **I** (Fig. 9) has been analyzed in terms of intra- and intermolecular hydrogen bonds. The MEP derived charges with density functional BLYP using DMol[3] program indicated strong negative charges on the oxygen (O1 and O2) and nitrogen (N1 and N2) atoms (**TABLE 6**). The amino nitrogen atom N2 carries the most negative charge due to electron donating nature of adjacent hydrogen atoms. The terminal hydrogen atoms of the amino group (H1N2 and H2N2) and the carboxyl group (H1O2) carry the most positive charge as they are adjacent to strong electronegative nitrogen and oxygen atoms, respectively. The C5 carbon atom being adjacent to both the pyridine (N1) and amino (N2) nitrogen atoms bears a strong positive charge. As a result of this redistribution of charges, the net dipole moment of **I** is 4.68 debye.

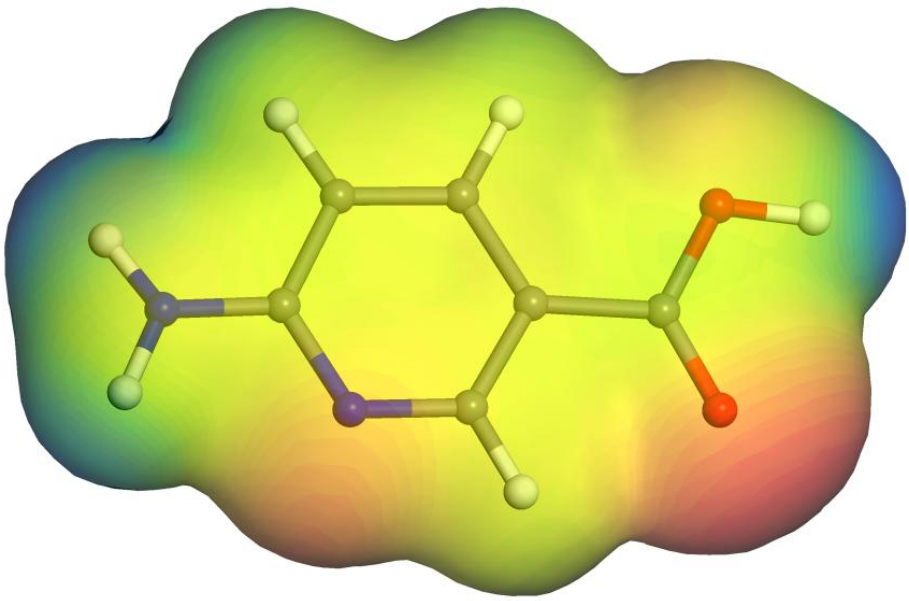

Fig. 9: MEP surface of $C_6H_6N_2O_2$ (I)

The electrostatic potential maxima and minima ($V_{s,max}$, $V_{s,min}$) associated with different donor and acceptor atoms serve as good indicators of hydrogen bond validation in **I**. The hydrogen atoms associated with the carboxyl group (H1O2) and amino group (H2N2 and H1N2) carry the most positive potential values of 71, 65 and 56 kcal/mol, respectively, and act as strong donors. The carbonyl oxygen atom O1 and pyridine nitrogen atom N1, correspond to the most negative potential values of -44 and -38 kcal/mol, respectively, and can act as strong acceptors. High values of $V_{s,max}$ and $V_{s,min}$ indicate very strong hydrogen bonding, which is consistent with the results (**TABLE 4**) obtained via crystallographic analysis.

Table 6: Table for ESP fitted charges in $C_6H_6N_2O_2$ (I)

Atom	charge (a.u.)	Atom	charge (a.u.)
C1	0.351	O1	-0.545
C2	-0.259	O2	-0.544
C3	0.117	H1	0.082
C4	-0.570	H3	0.119
C5	0.856	H4	0.199
C6	0.591	H1N2	0.396
N1	-0.696	H2N2	0.381
N2	-0.889	H1O2	0.412

ISSN- 2394-5125 VOL 7, ISSUE 06, 2020

3.5: Electronic structure

The frontier molecular orbitals HOMO (highest occupied molecular orbital), LUMO (lowest unoccupied molecular orbital), HOMO-1 (second highest occupied molecular orbital) and LUMO+1 (second lowest unoccupied state) of **I** are shown in Fig. 10, where colors on the isosurface are to distinguish the phase of the wave function. These frontier orbitals are the most involved states in electronic transitions.The HOMO can be thought of as the outermost orbital containing electrons and it tends to give these electrons and acts as an electron donor. On the other hand, the LUMO relates to the innermost orbital containing vacant place and represents the ability of electron accepting. The HOMO electrons are mostly localized on the C-N , C-C bonds of the aromatic ring, carbonyl oxygen O1, amino nitrogen N2 atoms, while the LUMO population prevails over the C2-C6 bond, C1, C3, C5, O1, O2 and N2 atoms showing anti bonding characteristics. Energy eigen values E_{HOMO} and E_{LUMO} in **I** are -5.36 and -1.80 eV, indicating a high energy difference of 3.56 eV between the two orbitals.

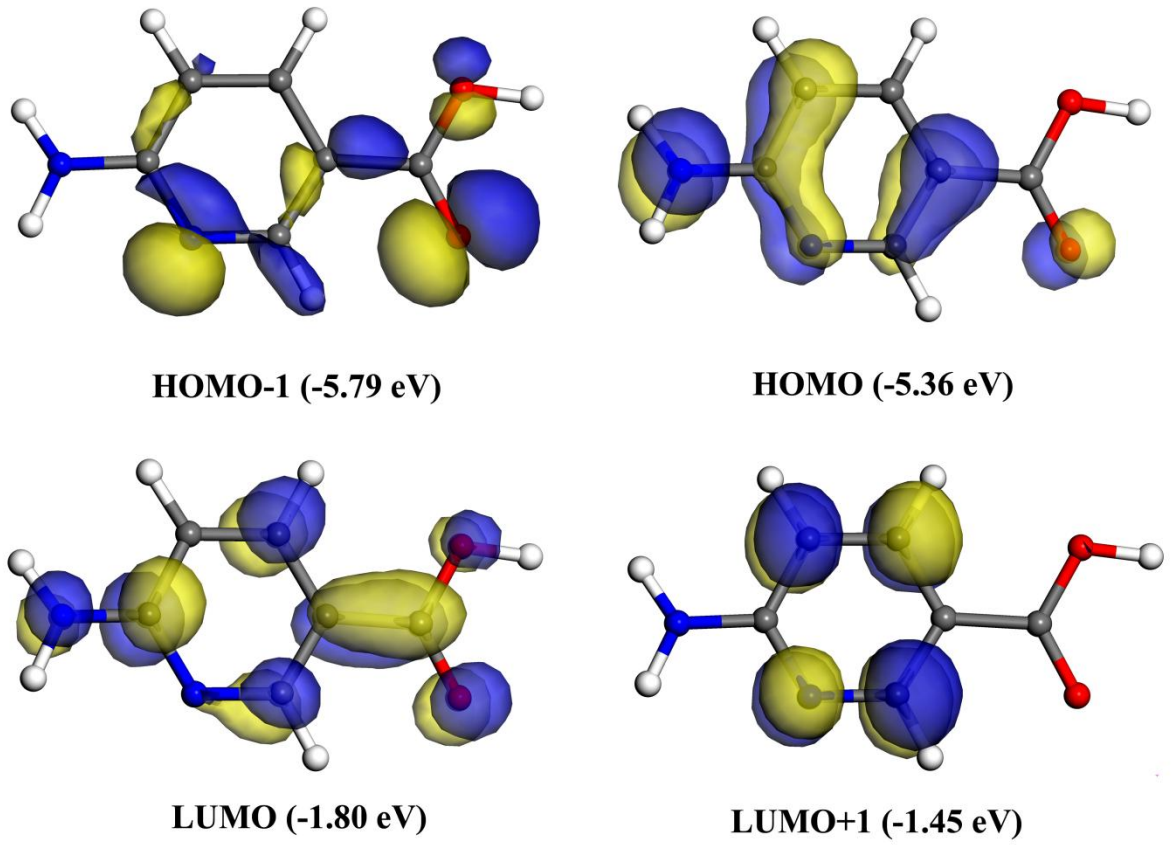

Fig. 6.10: Frontier molecular orbitals of $C_6H_6N_2O_2$ (I)

4: Conclusion

To summarize, crystal structure of 6-ANA (**I**) has been determined from synchrotron X-ray powder diffraction data using a sample containing more than one phases. As the sample contained small amount of NaCl as impurity, the structure of **I**could be solved and later quantitative phase analysis was carried out with 6-ANA as the major phase and NaCl as the minor phase (impurity). It might not have been possible if the impurity phase had strong peaks in the 2θ region of the first 20 peaks of 6-ANA used for indexing the pattern. The crystal packing of **I** has been illustrated by an interplay of N-H···O and O-H···N hydrogen bonds, which assemble molecules into a three-dimensional cage like structure via the formation of $R_2^2(8)$ rings and $C_2^2(16)$ polymeric chains. The results also emphasize that a reliable ranking of hydrogen bond donor strength in **I** can be achieved by using molecular electrostatic potential (MEP) surfaces and for competing hydrogen bond donors, the selection depends strongly on the MEP values of the acceptor. A comparison of relative contribution of different interactions to the Hirshfeld surfaces of **I** and a few NA derivatives indicated that H···H, N···H and O···H

ISSN- 2394-5125 VOL 7, ISSUE 06, 2020

interactions can account for almost 70% of the Hirshfeld surface area in these compounds. Finally, the present work clearly demonstrates the potential of PXRD for determining the crystal structure of organic materials even with more than one phase directly from the bulk powder without the need to grow single crystals provided the other phase(s) does not hamper the indexing part.

5. Acknowledgement

The authors are thankful to Dr. Surajit Banerjee and Dr. Bob VonDreele, ArgonneNational Laboratory, U.S.A. for availing the facility of synchrotron radiation.

References

[1] P. C. R. Soares-Santos, R. A. Sá Ferreira, T. Trindade, L. D. Carlos and H. I. S. Nogueira, Terbium(III) complexes of 2-aminonicotinic, thiosalicylic and anthranilic acids: synthesis and photoluminescence properties, J. All. Comp., 451, 2008, 575-577.

[2] S. K. Dogra, Solvatochromism and prototropism in 6-aminonicotinic acid, J. Lumin., 114, 2005, 213-226.

[3] M. Karabacak and M. Kurt,Comparison of experimental and density functional study on the molecular structure, infrared and Raman spectra and vibrational assignments of 6-chloronicotinic acid, Spectrochim. Acta Part A, 71, 2008, 876-883.

[4] M. Karabacak, M. Çınar and M. Kurt, An experimental and theoretical study of molecular structure and vibrational spectra of 2-chloronicotinic acid by density functional theory and ab initio Hartree–Fock calculations, J. Mol. Struct., 885, 2008, 28-35.

[5] J. P. Jasinski, R. J. Butcher, M. S. Siddegowda, H. S. Yathirajan and A. R. Ramesha, Etoricoxibium picrate,Acta Crystallogr. Sect. E, 67, 2011, o107-o108.

[6] D. Bardelang, F. Camerel, A. C. G. Hotze, B. Kariuki, B. Paik, M. Schmutz, R. Ziessel and M. J. Hannon, Sodium chains as core nanowires for gelation of organic solvents from a functionalized nicotinic acid and its sodium salt, Chem. Eur. J., 13, 2007, 9277-9285.

[7] W. C. J. Ross, Some 6-substituted nicotinamides: synthesis and antineoplastic activities, Biochem. Pharmacol., 16, 1967, 675-680.

[8] O. H. Johnson, D. E. Green and R. Pauli,The antibacterial action of derivatives and analogues of p-aminobenzoic acid, J. Biol. Chem., 153, 1944, 37-47.

[9] J. G. Wooley, M. K. Murphy, H. W. Bond and T. D. Perrine, The Effect of Certain Chemical Compounds on the Multiplication of T_2 Bacteriophage, J. Immun., 68, 1952, 523-530.

[10] R. Ramesh Raju, S. Krishna Mohan and S. Jayarama Reddy, Electroorganic synthesis of 6-aminonicotinic acid from 2-amino-5-chloropyridine, Tetrahedron Letters, 44, 2003, 4133–4135.

[11] A. J. Dobson and R. E. Gerkin, 2-Aminonicotinic AcidActa Crystallogr. Sect. C, 53, 1997, 1427-1429.

[12] M. Karabacak, E. Kose and A. Atac, Spectrochim. Molecular structure (monomeric and dimeric structure) and HOMO–LUMO analysis of 2-aminonicotinic acid: A comparison of calculated spectroscopic properties with FT-IR and UV–visActa Part A, 91, 2012, 83-96.

[13] W. I. F. David and K. Shankland, Structure determination from powder diffraction data Acta Crystallogr. Sect. A, 64, 2008, 52-64.

[14] V. Favre-Nicolin and R. Černý, : A better FOX: using flexible modelling and maximum likelihood to improve direct-space ab initio structure determination from powder diffraction Z. Kristallogr. - Cryst. Mat., 219, 2004, 847–856.

[15] S. Pagola, P. W. Stephens, D. S. Bohle, A. D. Kosar and S. K. Madsen, The structure of malaria pigment beta-haematin, Nature, 404, 2000, 307-310.

[16] K. D. M. Harris and E. Y. Cheung, How to determine structures when single crystals cannot be grown: opportunities for structure determination of molecular materials using powder diffraction data Chem. Soc. Rev., 33, 2004, 526-538.

[17] T. Dey, P. Chatterjee, A. Bhattacharya, S. Pal and A. K. Mukherjee, Three nimesulide derivatives: synthesis, ab initio structure determination from powder X-ray diffraction, and quantitative analysis of molecular surface electrostatic potential, Cryst. Growth Des., 16, 2016, 1442-1452.

[18] U. Das, J. Naskar and A. K. Mukherjee,Conformational analysis of an acyclic tetrapeptide: ab-initio structure determination from X-ray powder diffraction, Hirshfeld surface analysis and electronic structure, J. Pept. Sci., 21, 2015, 845-852.

[19] P. A. Williams, C. E. Hughes and K. D. M. Harris,L-Lysine: Exploiting Powder X-ray Diffraction to Complete the Set of Crystal Structures of the 20 Directly Encoded Proteinogenic Amino Acids Angew. Chem., Int. Ed., 54, 2015, 3973-3977.

[20] J.-B. Arlin, R. M. Bhardwaj, A. Johnston, G. J. Miller, J. Bardin, F. MacDougall, P. Fernandes, K. Shankland, W. I. F. David and A. J. Florence, Structure and stability of two polymorphs of creatine and its monohydrate, CrystEngComm, 16, 2014, 8197-8204.

[21] A. Altomare, C. Giacovazzo, A. Guagliardi, A. G. G. Moliterni, R. Rizzi and P.-E. Werner, New techniques for indexing: N-TREOR in EXPOJ. Appl. Crystallogr., 33, 2000, 1180-1186.

[22] A. Altomare, C. Cuocci, C. Giacovazzo, A. Moliterni, R. Rizzi, N. Corriero and A. Falcicchio, EXPO2013: a kit of tools for phasing crystal structures from powder data, J. Appl. Crystallogr., 46, 2013,1231-1235.

[23] P. Thompson, D. E. Cox and J. B. Hastings,Rietveld refinement of Debye-Scherrer synchrotron X-ray data from Al_2O_3, J. Appl. Crystallogr., 20, 1987, 79-83.

[24] J. J. P. Stewart,Optimization of parameters for semiempirical methods V: Modification of NDDO approximations and application to 70 elements J. Mol. Model., 13, 2007, 1173-1213.

[25] H. Rietveld, Line profiles of neutron powder-diffraction peaks for structure refinement, Acta Crystallogr., 22, 1967, 151-152.

[26] A. C. Larson and R. B. Von Dreele, General Structure Analysis System (GSAS), Los Alamos Laboratory Report, LAUR, 2000.

[27] P. L. Lee, D. Shu, M. Ramanathan, C. Preissner, J. Wang, M. A. Beno, R. B. Von Dreele, L. Ribaud, C. Kurtz, S. M. Antao, X. Jiao and B. H. Toby, A twelve-analyzer detector system for high-resolution powder diffraction, J. Synch. Rad., 15, 2008, 427-432.

[28] J. Wang, B. H. Toby, P. L. Lee, L. Ribaud, S. M. Antao, C. Kurtz, M. Ramanathan, R. B. V. Dreele and M. A. Beno, A dedicated powder diffraction beamline at the Advanced Photon Source: Commissioning and early operational results, Rev. Sci. Inst., 79, 2008, 085105.

[29] F. L. Hirshfeld, Bonded-atom fragments for describing molecular charge densities,Theoret. Chim. Acta, 44, 1977, 129-138.

[30] M. A. Spackman and D. Jayatilaka, Hirshfeld surface analysis, CrystEngComm, 11, 2009, 19-32.

[31] H. F. Clausen, M. S. Chevallier, M. A. Spackman and B. B. Iversen, Three new co-crystals of hydroquinone: crystal structures and Hirshfeld surface analysis of intermolecular interactions, New J. Chem., 34, 2010, 193-199.

[32] M. A. Spackman and J. J. McKinnon, Fingerprinting intermolecular interactions in molecular crystals, CrystEngComm, 4, 2002, 378-392.

[33] A. Parkin, G. Barr, W. Dong, C. J. Gilmore, D. Jayatilaka, J. J. McKinnon, M. A. Spackman and C. C. Wilson, Comparing entire crystal structures: structural genetic fingerprinting, CrystEngComm, 9, 2007, 648-652.

[34] A. L. Rohl, M. Moret, W. Kaminsky, K. Claborn, J. J. McKinnon and B. Kahr, Hirshfeld Surfaces Identify Inadequacies in Computation of Intermolecular Interactions in Crystals: Pentamorphic 1,8-Dihydroxyanthraquinone, Cryst. Growth Des., 8, 2008, 4517-4525.

[35] J. J. McKinnon, M. A. Spackman and A. S. Mitchell, Novel tools for visualizing and exploring intermolecular interactions in molecular crystals, Acta Crystallogr. Sect. B, 60, 2004, 627-668.

[36] S.K. Wolff, D.J. Grimwood, J.J. McKinnon, M.J. Turner, D. Jayatilaka, M.A. Spackman,Crystal Explorer 3.1, University of Western Australia, Perth, Australia, 2012.

[37] C. B. Aakeröy, T. K. Wijethunga and J. Desper, Molecular electrostatic potential dependent selectivity of hydrogen bonding, New J. Chem., 39, 2015, 822-828.

[38] P. Politzer and J. S. Murray, Quantitative analyses of molecular surface electrostatic potentials in relation to hydrogen bonding and co-crystallization, Cryst. Growth Des., 15, 2015, 3767-3774.

[39] A. D. Becke, Density-functional thermochemistry. III. The role of exact exchange, J. Chem. Phys., 98, 1993, 5648-5652.

[40] C. Lee, W. Yang and R. G. Parr, Development of the Colle-Salvetti correlation-energy formula into a functional of the electron density, Phys. Rev. B, 37,1988, 785-789.

[41] B. Delley, An all-electron numerical method for solving the local density functional for polyatomic molecules, J. Chem. Phys., 92, 1990, 508-517.

[42] A. Tkatchenko and M. Scheffler, Accurate Molecular Van Der Waals Interactions from Ground-State Electron Density and Free-Atom Reference Data, Phys. Rev. Lett., 102, 2009, 073005.

[43] R. F. W. Bader, M. T. Carroll, J. R. Cheeseman and C. Chang, Properties of atoms in molecules: atomic volumes, J. Am. Chem. Soc., 109, 1987, 7968-7979.

[44] A. Kutoglu and C. Scheringer, Nicotinic acid, $C_6H_5NO_2$: refinement, Acta Crystallogr. Sect. C, 39, 1983, 232-234.

[45] A. Zafar, S. J. Geib, Y. Hamuro, A. J. Carr and A. D. Hamilton, Hydrogen bonding control of molecular self-assembly: Aggregation behavior of acylaminopyridine-carboxylic acid derivatives in solution and the solid state, Tetrahedron, 56, 2000, 8419-8427.

[46] M.-L. Pan, Y.-H. Luo and S.-L. Mao, 6-Methylnicotinic acid, Acta Crystallogr. Sect. E, 67, 2011, o2345.

[47] C. Jelsch, K. Ejsmont and L. Huder, The enrichment ratio of atomic contacts in crystals, an indicator derived from the Hirshfeld surface analysis, IUCrJ, 1, 2014, 119-128.